A distinct isoform of Msp300/Nesprin organizes the perinuclear microtubule organizing center in adipose cells

Running title: An Msp300 isoform controls the MTOC in adipose cells

Garret M. Morton[1], Maria Pilar Toledo[1], Yiming Zheng[2], Chunfeng Zheng[1], Timothy L. Megraw[1]

[1]Department of Biomedical Sciences, Florida State University, Tallahassee, FL, USA

[2]State Key Laboratory of Cellular Stress Biology, School of Life Sciences, Faculty of Medicine and Life Sciences, Xiang'an Hospital of Xiamen University, Xiamen University, Xiamen, China, 361102, and Shenzhen Research Institute of Xiamen University, Shenzhen, China, 518057

Correspondence:

timothy.megraw@med.fsu.edu

Abstract

In many cell types, disparate non-centrosomal microtubule-organizing centers (ncMTOCs) replace functional centrosomes and serve the unique needs of the cell types in which they are formed. In *Drosophila* fat body cells (adipocytes), an ncMTOC is organized on the nuclear surface. This perinuclear ncMTOC is anchored by Msp300, encoded by one of two Nesprin-encoding genes in *Drosophila*. Msp300 and the spectraplakin short stop (shot) are co-dependent for localization to the nuclear envelope to generate the ncMTOC where they recruit the microtubule minus-end stabilizer Patronin (CAMSAP). The fat body perinuclear ncMTOC requires Patronin, Ninein, and Msps (ortholog of ch-TOG), but does not require γ-tubulin for MT assembly. The *Msp300* gene is complex, encoding at least eleven isoforms. Here we show that two Msp300 isoforms, Msp300-PE and -PG, are required and only one, Msp300-PE, appears sufficient for generation of the ncMTOC. Loss of Msp300-PE,-PG retains the presence of the other isoforms at the nuclear surface, indicating that they are not sufficient to generate the ncMTOC. Loss of Msp300-PE,-PG results in severe loss of localization of shot and Patronin, and disruption of the MT array. This results in nuclear mispositioning and loss of endosomal trafficking. Msp300-PE has an unusual domain structure including a lack of a KASH domain and very few spectrin repeats and appears therefore to have a highly derived function suited to generating an ncMTOC on the nuclear surface.

Introduction

The linker of nucleoskeleton and cytoskeleton (LINC) complex spans the nuclear envelope and provides a physical connection between the nuclear interior and the cytoplasm and plasma membrane [1]. Reflecting the essential roles of the LINC complex in cell function, mutations in LINC complex proteins are associated with genetic diseases [2, 3] including muscular dystrophies [4, 5], cardiomyopathies [6, 7], cerebellar ataxia [8, 9], and arthrogryposis [10]. The LINC complex is integral to cellular processes such as DNA damage response [11, 12], meiotic chromosome movement [13, 14], mechanosensation [1], and nuclear positioning and anchoring [2, 15-17]. Comprising the LINC complex are SUN (Sad1/UNC-84 homology) and KASH (Klarsicht/ANC-1/Syne homology) proteins. SUN proteins reside at the inner nuclear membrane and contain an N-terminus that extends into the nucleoplasm, where it interacts with lamins of the nucleoskeleton and other nucleoplasm proteins, while the C-terminal SUN domain forms contacts with KASH proteins in the perinuclear space. The KASH proteins reside on the outer nuclear membrane, associate with cytoskeletal components, and are characterized by a C-terminal KASH domain that associates with the SUN domain of the SUN proteins within the internuclear space.

In *Drosophila*, the LINC complex components include two KASH proteins, Klarsicht (Klar) and Muscle-specific protein 300 kDa (Msp300), and one primary SUN protein, Klaroid (Koi), while a second SUN protein, Spag4, is expressed in the testes. The *Drosophila* LINC proteins are responsible for the proper positioning of muscle myonuclei [18], similar to their roles in vertebrate muscle [5, 19-21]. Msp300, which was first identified in the muscle [22], promotes myonuclear spacing [23]. These findings indicate a role for nuclear mispositioning in the pathogenesis of diseases such as Emery-Dreifuss muscular dystrophy (EDMD) [23, 24]. As seen with other nuclear envelope spectrin repeat proteins (Nesprins), Msp300 contains calponin homology (CH) domains, numerous spectrin repeats (SR), and a C-terminal KASH domain. In addition, *Msp300* encodes at least eleven isoforms of various molecular weights expressed from multiple promoters and with alternative mRNA splicing and transcription termination (Figure 1). Furthermore, subsets of these isoforms have been shown to exhibit unique functions. In the muscle, isoforms containing the CH domains but lacking the KASH domain were found to contribute to muscle function and Z-line organization, while isoforms lacking the CH domains but containing the KASH domain were shown to be responsible for maintaining myonuclear positioning [25].

In *Drosophila* fat body cells, which are functionally comparable to mammalian adipocytes and liver cells, Msp300 establishes a perinuclear non-centrosomal microtubule organizing center (ncMTOC) at the nuclear surface that controls microtubule organization, nuclear positioning, and endocytic vesicle trafficking [26]. Notably, Klar and Koi were not required for organization of this ncMTOC. Here, we have identified one particular and distinct isoform of Msp300 that is responsible for organization of the perinuclear ncMTOC in the fat body. By utilizing deletion mutants, transposable element insertion mutations, and RNAi, we show that one unconventional isoform, Msp300-PE, appears sufficient for establishment of the ncMTOC on the nuclear surface.

55 # Results

56 **The Msp300 locus is complex**

57 The *Msp300* gene is complex, encoding at least 11 isoforms ranging in size from 47 to 1,500 kDa
58 (Fig 1A). These variants arise from alternative promoters, mRNA splice sites, and transcriptional

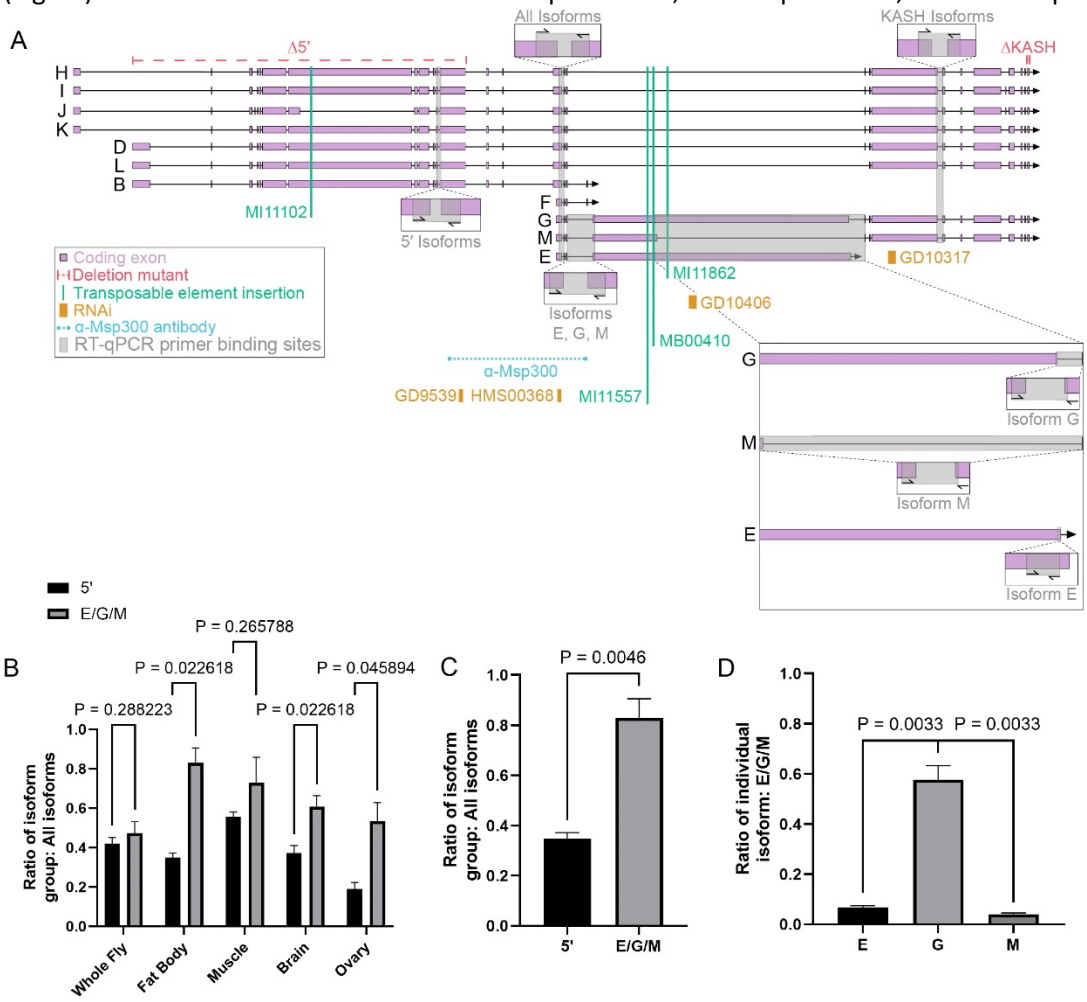

59

Figure 1. *Msp300* gene isoforms and genetic analysis features. (A) Schematic of the isoforms expressed from the *Msp300* gene. To probe the function of different isoforms at the fat body perinuclear MTOC, a combination of deletion mutants (red), transposable element insertion mutations (green), and RNAi (orange) were used. The isoforms and regions of these isoforms targeted by the various lines are depicted. The epitope recognized by the α-Msp300 antibody (blue) is shown. Binding sites of the primers for RT-qPCR are represented by the magnified views of the exons. (B) Bar graph comparing the expression levels of isoforms groups relative to all isoforms in different tissues as determined by RT-qPCR. RNA was isolated from whole adult flies, adult flight muscles, adult ovaries, larval fat bodies, and larval brains. The RNA extraction from each tissue was performed in triplicate and each RT-qPCR reaction was run in triplicate. Expression of Msp300 isoforms was normalized to the GPDH1 and α-Tubulin reference genes. (C) In the fat body, Isoforms E, G, and M were found to be more highly expressed than the 5' isoforms. (D) Individual expression levels of isoforms E, G, and M relative to the expression level of all three isoforms in the fat body.

terminators. From available expression data it is evident that isoforms B, E, and F lack the KASH domain, and isoforms E, F, G, and M lack CH domains. Isoforms E and M encode only two spectrin repeats, compared to most other isoforms that contain 20-52 spectrin repeats. In addition, isoforms E, G, and M include all or part of a large, unique exon that is not found in the other isoforms.

A set of isoforms are expressed more highly in the fat body

We used reverse transcription quantitative PCR (RT-qPCR) to assess the levels of expressed mRNAs of groups of Msp300 isoforms in different tissues, including whole body, brain, flight muscle, ovary and fat body. We designed PCR primers to differentiate between amplification of the target cDNAs and off-target genomic DNA and to quantify the relative levels of expression of the different isoforms. We assessed expression of three sets of isoforms: all isoforms, those expressed from the two most 5' promoters, and the E/G/M group of isoforms (Fig 1A). These data show that Msp300 is expressed in all tissue types tested (Fig 1B). In the fat body, E/G/M are more highly expressed than the 5' isoforms, with isoform G exhibiting the highest expression level of the E/G/M group (Fig 1C-D).

Isoform E is sufficient for the fat body ncMTOC

To examine which protein isoforms of Msp300 are expressed and localized to the nuclear envelope in fat body cells, we used RNAi to knock down expression of clusters of isoforms and stained with a polyclonal Msp300 antibody that targets all isoforms (Fig 1A) to detect remaining isoforms at the nuclear envelope. We generated tissue mosaics of RNAi knockdown using the coinFLP system [27]. With coinFLP, we obtained mosaic tissues where RNAi knockdown cells are present together with control cells. The RNAi knockdown clones are differentiated from the control cells by co-expression of nuclear-targeted mCherry (mCherry-nls) in the clones.

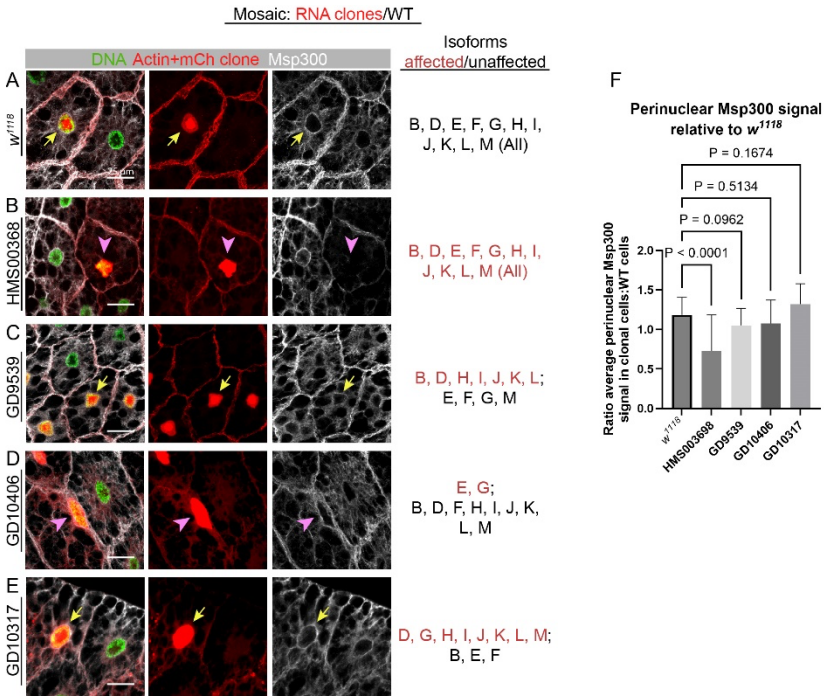

Figure 2. Multiple Msp300 isoforms localize to the nuclear surface. Immunostaining of fat bodies for Msp300 in *w*^{1118} (A) or following RNAi knockdown by the HMS00368 (B), GD9539 (C), GD10406 (D), or GD10317 (E) RNAi lines. Mosaic expression was achieved using the coinFLP system. Clonal RNAi knockdown cells express nuclear mCherry (red). Nuclei were stained with DAPI and pseudo-colored green. Isoforms targeted by each RNAi line are indicated. Clones characterized by nuclear mispositioning are denoted by a pink arrowhead, while clones with properly positioned nuclei are denoted by a yellow arrow. (F) Quantitation of perinuclear Msp300 localization.

To demonstrate that the clones do not exhibit inherent defects in perinuclear Msp300 localization or nuclear positioning,

83 w^{1118} was used as a control (Fig 2A, F). When all Msp300 isoforms were knocked down (with HMS00368
84 [28]), the perinuclear Msp300 signal was significantly reduced compared to the control cells, as expected

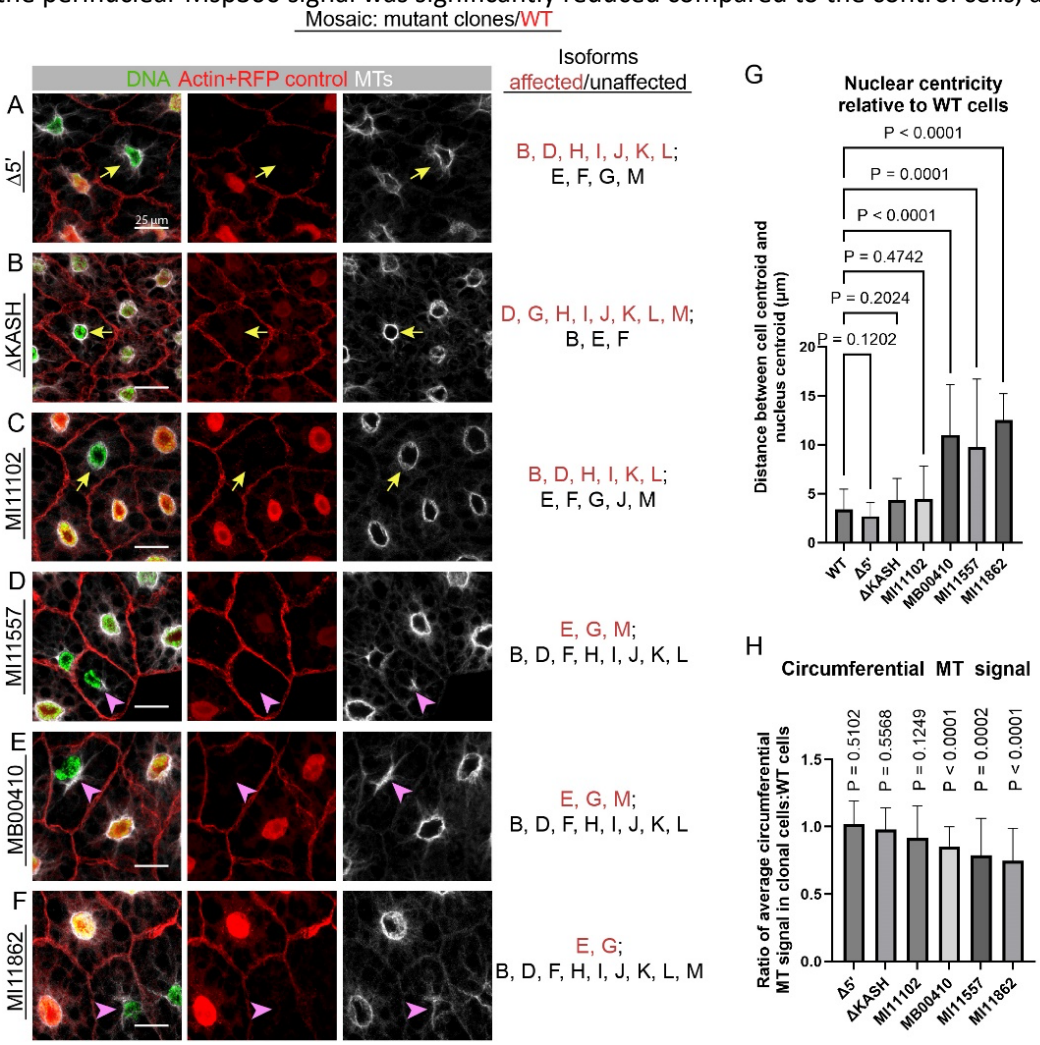

Figure 3. Msp300 isoforms E and G are required for nuclear positioning and microtubule organization. Nuclear positioning and MT organization was assessed by immunostaining fat bodies containing mosaic clones of Δ5′ (A), ΔKASH (B), MI11102 (C), MI11557 (D), MB00410 (E), and MI11862 (F) Msp300 mutants. The FLP-FRT system was used to generate mutant clones, where WT alleles are distinguished by the expression of nuclear RFP. The isoforms affected by each mutant allele are listed (red text). Normal nuclear positioning and MT organization is represented by a yellow arrow, while mispositioned nuclei with disrupted MT organization are indicated with a pink arrowhead. Disruption of isoforms essential to the MTOC results in the loss of nuclear centricity (G) and the diminishment of circumferential MTs (H).

85 (Fig 2B, F). Consequentially, the nuclei were mispositioned, a phenotype shown previously for *Msp300*
86 knockdown, and which is associated with the loss of microtubule organization at the nuclear surface
87 [26]. In contrast, targeting of the 5′ isoforms (with GD9539 [29]) does not diminish Msp300 localization
88 to the nuclear surface (Fig 2C, F). Knockdown of isoforms E and G (with GD10406 [29]) results in nuclear
89 mispositioning, and the Msp300 signal at the nuclear envelope is significantly reduced (Fig 2D, F). The
90 persistence of signal at the nuclear envelope is likely contributed by the other isoforms not targeted by
91 RNAi. Meanwhile, knockdown of all KASH-containing isoforms (with GD10317 [29]), which includes G,

does not significantly reduce perinuclear Msp300 (Fig 2E, F) and did not affect nuclear positioning. The presence of Msp300 signal at nuclei following knockdown of each set of transcripts is consistent with the RT-qPCR data showing that most Msp300 isoforms are expressed in the fat body. Importantly, the loss of nuclear positioning while retaining Msp300 signal upon knockdown of the E/G isoforms indicates that these isoforms are uniquely required for nuclear positioning, likely through the regulation of MT organization.

Msp300 isoform E is sufficient for nuclear positioning and microtubule organization, with probable involvement of Isoform G

Drosophila fat body cells are characterized by a nucleus positioned at the center of the cell and MTs organized at the nuclear surface that radiate outwards and connect the nucleus to the plasma membrane. Specifically, two classes of MTs are present within the cell. Circumferential MTs surround the nucleus, while radial MTs extend from the nucleus into the cytoplasm. Knockdown of all isoforms of Msp300 in the fat body results in nuclear mispositioning and loss of MT organization due to the requirement of Msp300 at the fat body ncMTOC [26]. To determine which isoforms are required to maintain nuclear positioning and MT organization, we used a variety of mutant lines in addition to the RNAi lines used in Figure 2. These mutants were analyzed as mosaic homozygous mutant clones using the FLP-FRT recombination system [30] to generate mosaic clones in which control cells express nuclear RFP while clonal mutant cells do not (Fig 3).

First, we examined a deletion mutant that deletes the 5' end of the gene [31], disrupting isoforms B, D, H, I, J, K, and L, and a second deletion mutant that deletes the sequences encoding the

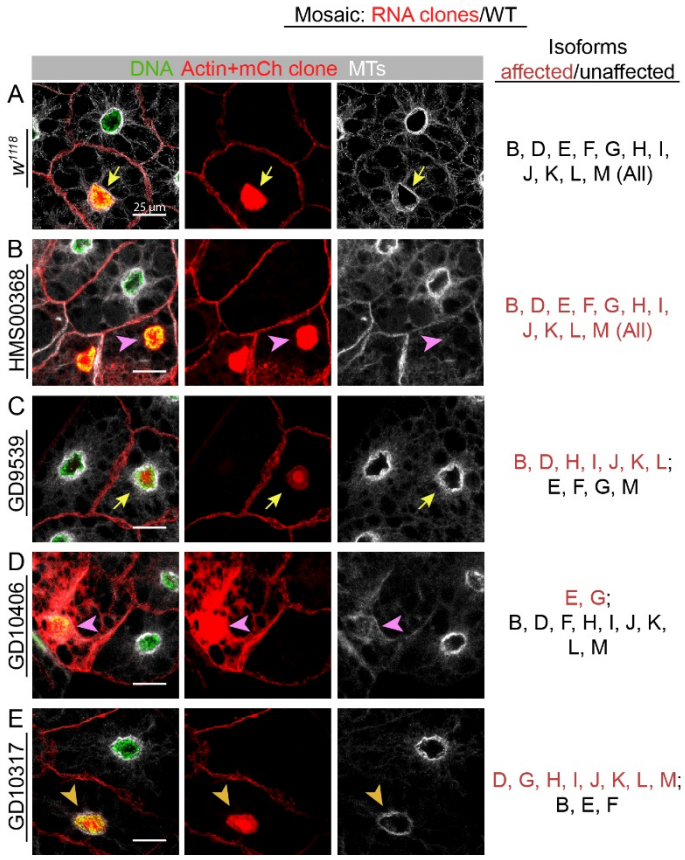

Figure 4. The perinuclear ncMTOC is organized by isoforms E and G. Fat bodies were analyzed by immunofluorescence microscopy to determine the effects of w^{1118} (A), as well as the HMS00368 (B), GD9539 (C), GD10406 (D), and GD10317 (E) RNAi lines on nuclear positioning and MT organization. RNAi lines were expressed with the coinFLP system, where knockdown clones are marked with nuclear mCherry. Isoforms targeted by each line are shown to the right of each group of microscopy images with red text. RNAi knockdown cells with properly positioned nuclei and organized radial and circumferential MTs are indicated (yellow arrows). Knockdown of isoforms required at the MTOC results in mispositioning of nuclei and loss of MT organization (pink arrowhead). Knockdown with GD10317 shows a hypomorphic phenotype characterized by reduced MTs in the absence of nuclear mispositioning (gold arrowheads).

112 KASH domain [32] (see Fig 1A). In both cases, nuclear positioning and MT organization were unaffected,
113 indicating that the 5′ isoforms and also the KASH domain are not required for generating the ncMTOC
114 (Fig 3A-B, G-H). Next, we used lines containing transposable element insertions within *Msp300* exons
115 that generate truncation mutations (see Fig 1A). Consistent with the 5′ deletion, the MI11102 [33]
116 transposon insertion within a coding exon near the 5′ end did not result in any changes to nuclear
117 positioning or MT organization (Fig 3C, G-H), further supporting that all isoforms encoded by exons in the
118 5′ half of the gene are not required for generation of the ncMTOC. In contrast, truncation of isoforms E,
119 G, and M by MI11557 [33] and MB00410 [34], or just E and G by MI11862 [33], results in severe nuclear
120 mispositioning and disruption of both radial and circumferential MTs (Fig 3D-F, G-H). These data show
121 that these isoforms, or at least the coding regions downstream of these three transposon insertion lines,
122 are necessary for proper function of the ncMTOC and truncation of isoforms E and G significantly impairs
123 the fat body ncMTOC. In addition, the expression of isoform M is not sufficient to support the ncMTOC.
124 We conclude from these mutant analyses that Msp300 isoforms E and G are required to generate the
125 ncMTOC on the fat body nuclear surface.

126 In addition to targeting sets of isoforms with mutant lines, we also used RNAi to knock down sets
127 of isoforms. An advantage afforded by RNAi is that it targets mRNAs for destruction, whereas the
128 transposon insertion mutants can conceptually result in the expression of truncated proteins. We used
129 the RNAi lines shown in Figures 1 and 2, and again generated mosaic knockdown with the coinFLP
130 system, but in these experiments we assessed MT organization and nuclear positioning rather than
131 Msp300 expression. First, we compared wild type (w^{1118}) to the internal control cells (Fig 4A) The
132 HMS00368 line depletes all Msp300 isoforms and resulted in severe nuclear mispositioning and MT
133 disruption as shown previously [26] (Fig 4B). Knockdown of the isoforms expressed from the 5′ region of
134 the gene did not affect nuclear positioning or MT organization (Fig 4C), consistent with the lack of
135 phenotype from mutants that affect the 5′ isoforms as shown in Figure 3. When targeting isoforms E and
136 G with GD10406, however, we observed mispositioned nuclei and disorganized MTs (Fig 4D). This result
137 indicates that isoforms E and/or G are required to organize the ncMTOC. However, knockdown of
138 isoform G and other isoforms containing the KASH domain using the GD10317 RNAi line resulted in a
139 hypomorphic phenotype characterized by cells with relatively weak MTs but that retain properly
140 positioned nuclei (Fig 4E). This absence of nuclear mispositioning, along with incomplete MT disruption,
141 suggests that isoform G supports but is not essential for the ncMTOC. We further show that when all
142 isoforms except isoforms E and F are knocked down by RNAi (by expressing GD9539 and GD10317
143 together), the ncMTOC remains intact, whereas expression of Msp300-PF alone is not sufficient (Fig S1).
144 Together, the results from the mutants and the RNAi lines show that, while isoform G plays a
145 contributing role in MT organization, isoform E appears sufficient to generate the perinuclear ncMTOC.

146 **<u>Retrograde endocytic vesicle trafficking is dependent on Msp300 isoform E</u>**

147 In addition to nuclear positioning and MT organization, we assessed the effects of Msp300
148 isoform depletion on endosome trafficking. Prior work showed that Msp300 is required for the ncMTOC
149 to organize MTs that support retrograde dynein-dependent endocytic vesicle trafficking [26]. In wild-type
150 cells, Rab5 endosomal vesicles are at the highest density near the plasma membrane and perinuclearly,
151 and disruption of MTs or dynein results in a loss of Rab5 endosome trafficking to the nuclear periphery
152 [26]. To test the involvement of Msp300 isoforms in endocytic vesicle localization, we imaged
153 endosomes marked with GFP-Rab5. In the w^{1118} control cells and cells expressing $RFP^{HMS05713}$ (RNAi
154 control), Rab5 vesicles comprise a perinuclear population forming a halo-like pattern (Fig 5A).

155 Knockdown of Patronin causes impaired retrograde trafficking, as seen by the loss of the perinuclear
156 Rab5 signal (Fig 5C). Similarly, the knockdown of all isoforms using HMS00368 results in a diminished
157 Rab5 population at the nuclear surface (Fig 5D). Depletion of the 5' isoforms from knockdown with

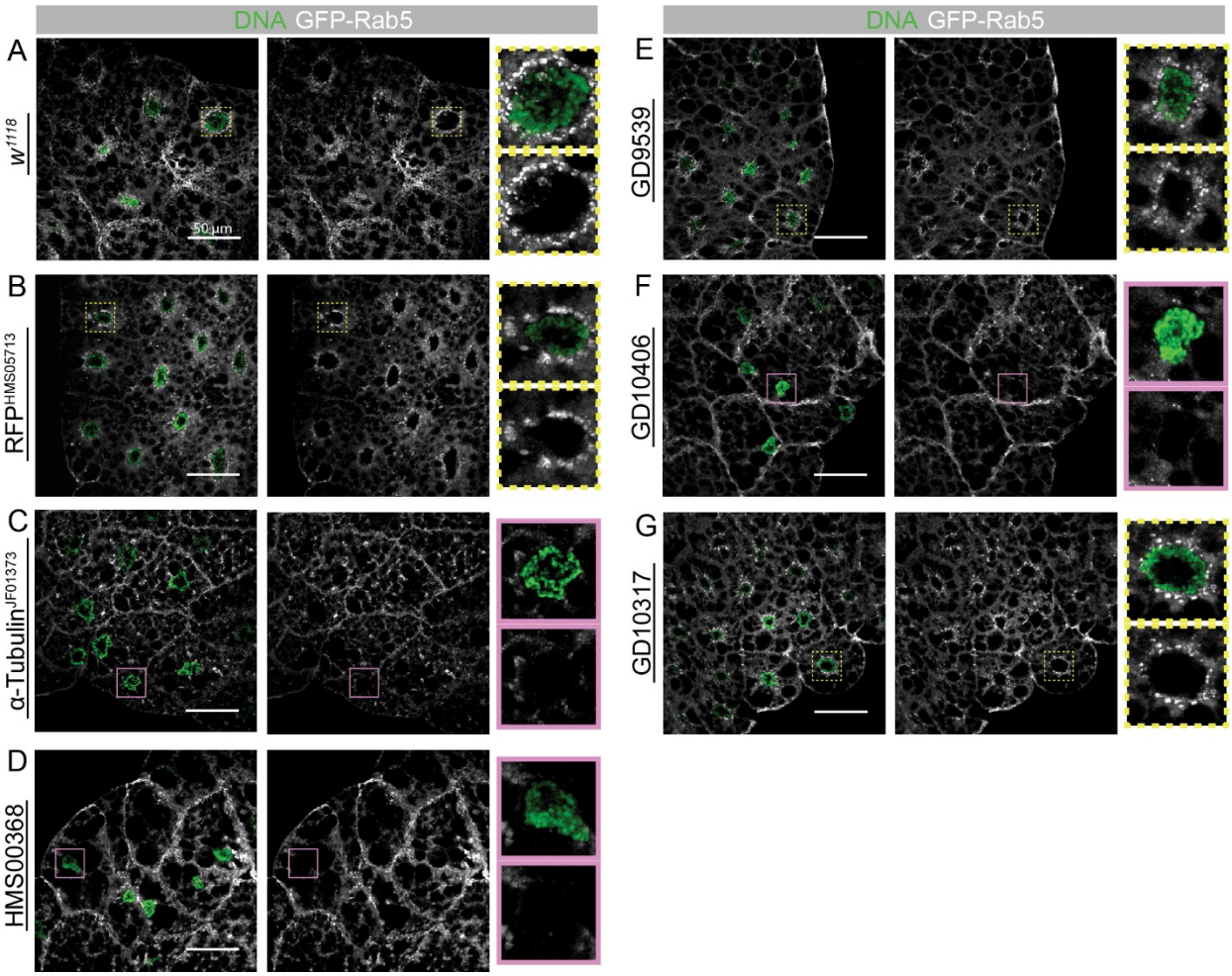

Figure 5. Msp300 isoforms E+G are required for retrograde trafficking of endocytic vesicles. Analysis of retrograde endosome trafficking in *w*^{1118} (A) cells, RFP^{HMS05713} (B), and α-Tubulin^{JF01373} (C), as well as in cells expressing the HMS00368 (D), GD9539 (E), GD10406 (F), and GD10317 (G) RNAi lines. RNAi was expressed throughout the entire fat body tissue with SPARC-GAL4. Images were captured using the same parameters to allow for direct comparison between samples. Insets show a magnified view of a single nucleus (green) and the perinuclear population of Rab5 endosomes (white). Control or unaffected cells exhibit a halo-like pattern of endocytic vesicles surrounding the nucleus (yellow dashed boxes), while knockdown of Msp300 isoforms essential for the MTOC causes loss of this signal (pink boxes).

158 GD9539 did not impact Rab5 signal, indicative of proper endosome trafficking (Fig 5E). In contrast,
159 knockdown of isoforms E and G with GD10406 resulted in low perinuclear GFP-Rab5 endosome signal
160 (Fig 5F). The knockdown of Isoform G and other KASH-containing isoforms via GD10317 did not
161 appreciably reduce the perinuclear GFP-Rab5 signal (Fig 5G). Together, these results further support that
162 isoform E is sufficient for ncMTOC function to support endosomal vesicle trafficking in the fat body.

163 **<u>Msp300 isoform E is required for the recruitment of the ncMTOC components shot and Patronin</u>**

To further evaluate the role of Msp300 isoforms at the fat body ncMTOC, we examined their dependence on the recruitment of other ncMTOC components. Msp300 recruits other components of the perinuclear ncMTOC including the spectraplakin short stop (shot) and the microtubule minus-end stabilizer Patronin [26, 35]. In the *w*^{1118} control, shot localizes to the nuclear surface, along MTs, and on the plasma membrane (Fig 6A). When Msp300 is completely knocked down, shot no longer localizes to the nuclear surface [26]. Consistently, we observed a decrease in the amount of Shot at the nuclear surface when we used HMS00368 to knock down all isoforms (Fig 6B). The knockdown does not, however, affect the presence of shot at the plasma membrane. Knockdown of the 5' isoforms (with GD9539) did not affect the perinuclear localization of shot (Fig 6C). Targeting of isoforms E and G with GD10406, on the other hand, causes a loss of shot from the nuclear surface (Fig 6D), while knockdown of the KASH isoforms that include Isoform G did not significantly impair shot localization (Fig 6E). These results indicate that Msp300 isoform E is sufficient for the recruitment of shot to the ncMTOC, consistent with our results showing its role in establishing the perinuclear ncMTOC.

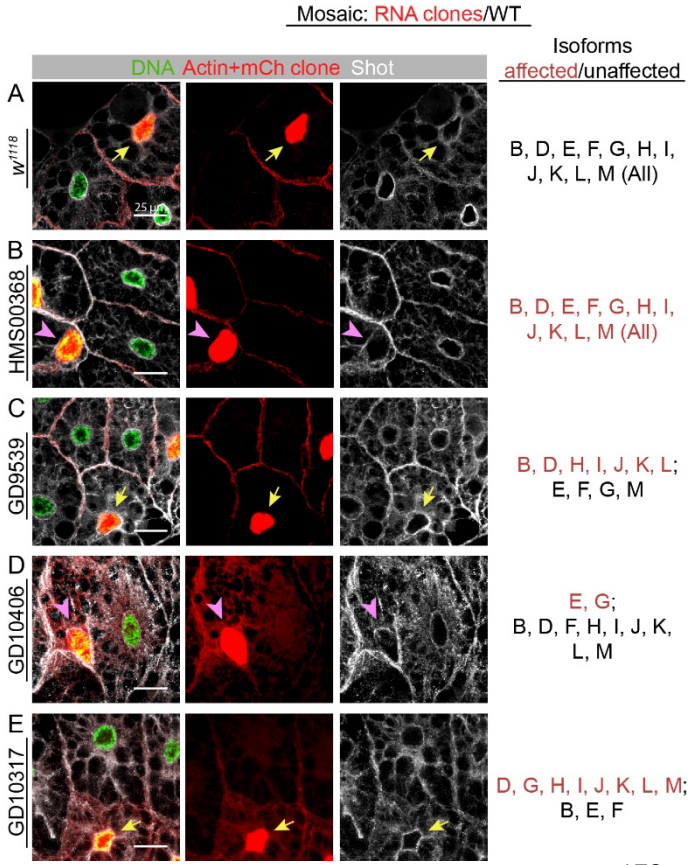

Figure 6. Localization of shot to the ncMTOC requires isoform E. Fat bodies were stained for shot in mosaic tissues expressing *w*^{1118} (A), HMS00368 (B), GD9539 (C), GD10406 (D), or GD10317 (E). The coinFLP system was used to express the RNAi, marked with co-expression of nuclear mCherry (red). Recruitment of shot to the nuclear surface by Msp300 results in a perinuclear shot signal (yellow arrows), while the knockdown of necessary Msp300 isoforms causes the loss of this signal (pink arrowheads).

Finally, we investigated the contribution of the isoforms to the recruitment of the CAMSAP homolog Patronin to the ncMTOC. Patronin is a MT minus-end stabilizer and a major regulator of MTs at the fat body perinuclear ncMTOC and complete Msp300 knockdown results in the loss of Patronin localization at the nuclear surface [26]. In *w*^{1118} control and Luciferase^{JF01355} cells expressing Patronin-GFP, Patronin localizes to the nuclear surface (Fig 7A-B, H), while in Patronin^{HMS01547} perinuclear Patronin is significantly reduced (Fig 7C, H).Depletion of all isoforms (with HMS00368) results in a significant decrease in the perinuclear localization of Patronin (Fig 7D, H). Knockdown of the 5' isoforms, in contrast, does not affect the presence of Patronin at the nuclear surface (Fig 7E, H). Patronin perinuclear localization is diminished when Isoforms E and G are knocked down with GD10406 but not when the 3' KASH-containing isoforms are knocked down (Fig 7D-E, H), consistent with the role for isoform E in MT organization and shot recruitment to the nuclear surface. Together, these data further support that

Msp300 isoform E is necessary and may be sufficient for MTOC generation through the recruitment of shot and Patronin.

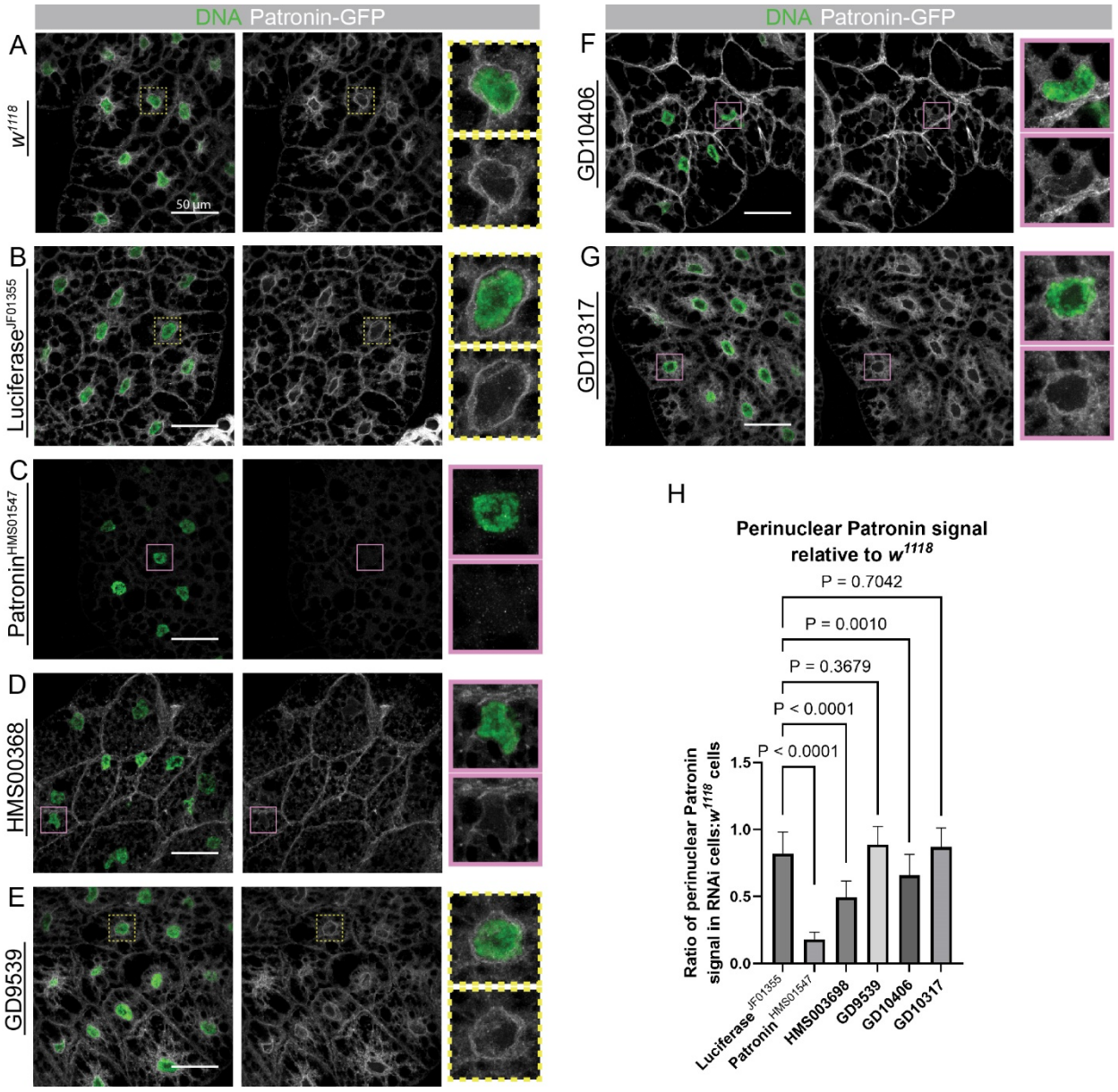

Figure 7. Patronin localization to the ncMTOC requires isoform E. Patronin localization in *w*^{1118} (A), Luciferase^{JF01355} (B), and Patronin^{HMS01547} (C) fat bodies and fat bodies expressing the HMS00368 (D), GD9539 (E), GD10406 (F), or GD10317 (G) RNAi lines. RNAi lines were expressed throughout the fat body with SPARC-GAL4. The same parameters were used to capture the images for each sample. Nuclei (DAPI, green) and Patronin-GFP (white). Patronin normally localizes perinuclearly (yellow dashed boxes). Knockdown of Msp300 isoforms essential for the ncMTOC results in loss of Patronin signal at the nuclear surface (pink boxes). (H) Remaining perinuclear Patronin signal in each sample represented in the form of a bar graph.

199 **Msp300-PE lacks a KASH domain and has two novel large tandem repeats**

200 Most cell types do not generate an MTOC on the nuclear surface, and fat body cells appear to
201 utilize a special isoform of Msp300, Msp300-PE to assemble it. To further investigate Msp300-PE to
202 understand what makes it unique, we analyzed its sequence and predicted domain structure with *in*
203 *silico* analysis tools. Nesprins characteristically consist of many spectrin repeats (SRs), a pair of calponin
204 homology (CH) domains, and a KASH domain [36]. The KASH domain consists of a transmembrane helix
205 and a short C-terminal region that resides in the internuclear space [37]. The giant Nesprin isoforms,
206 Nesprin-1 (1.0 MDa) and Nesprin-2 (0.8 MDa), contain 74 and 56 SRs, respectively [38, 39]. Similarly, one
207 of the largest Msp300 isoforms, Msp300-PD (1.41 MDa), contains 52 SRs, as well as 2 CH domains and a
208 KASH domain (Fig 8A) [40]. (Fig 8B). Msp300-PG (1.5 MDa), which also contributes to the MTOC,
209 contains no CH domains, 21 SRs, and a KASH domain. In contrast to the typical Nesprin domain structure,
210 Msp300-PE (1.06 MDa) contains no CH domains and has only 2 SRs (Fig 8C). Isoform E lacks a KASH
211 domain but is predicted to have a transmembrane domain at its C-terminus (Fig 8D), followed by a 35 aa
212 unstructured region. Msp300-PE contained no other predicted domains besides the SRs and the
213 transmembrane domain but, intriguingly, encodes two unique types of novel tandem repeat regions (Fig
214 8C), identified using the XSTREAM algorithm [41]. The first type, "Type 1," consists of ~20 copies of a
215 108-amino acid sequence that is remarkably similar among the tandem repeats (Fig 8E). "Type 2"
216 repeats also have a high degree of identity and consist of 101 amino acids repeated ~5-7 times in three
217 clusters (labeled 2A-2C in Figure 8C) with a total of ~19 repeats. Both types of repeats are predicted to
218 be largely unstructured but with some repeats forming parallel β-sheets. These repeat domains have no
219 previously described function.

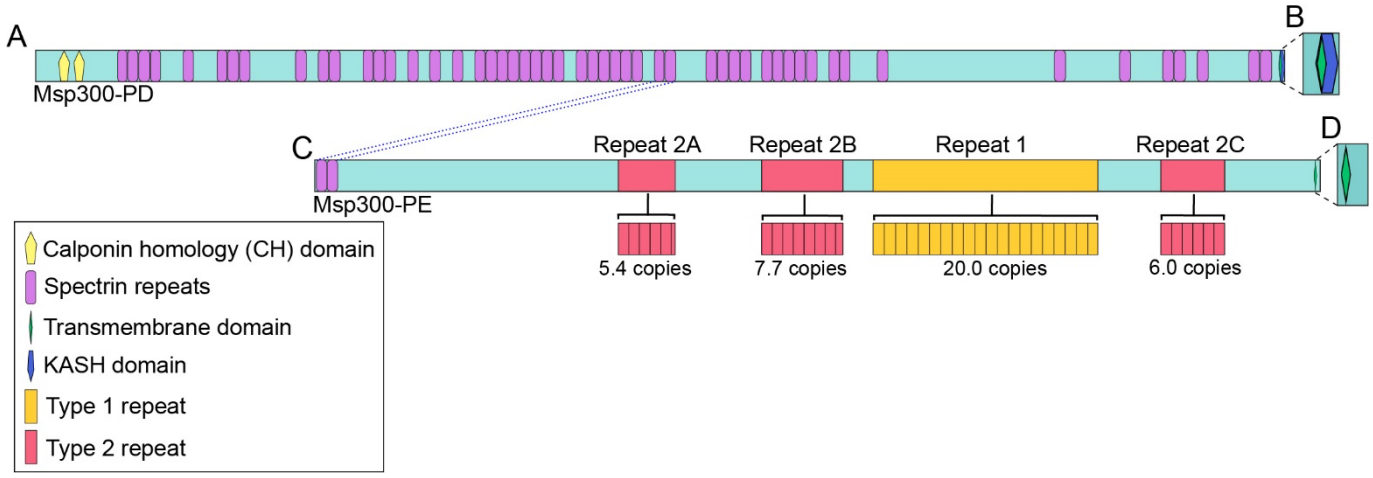

220

Figure 8. Msp300-PE is KASH-less and contains two novel large tandem repeats. (A-D) Schematic representations of Msp300-PD, a 'conventional' Nesprin, and Msp300-PE. Nesprins and most Msp300 isoforms such as PD (A) characteristically contain calponin homology domains, numerous spectrin repeats, and a KASH domain associated with a transmembrane domain (B). The atypical Msp300-PE (C) lacks calponin homology domains and contains only two spectrin repeats. The majority of Msp300-PE is comprised of two types of tandem repeats. Isoform PE also contains a transmembrane domain but lacks a KASH domain (D). Repeat 1 consists of a 107-amino acid sequence repeated 20 times. Repeat 2 consists of a different 101-amino acid sequence repeated at least 19 times among 3 clusters.

Discussion

Here we show that a unique isoform of Msp300, Msp300-PE, is necessary in fat body cells to organize the ncMTOC on the nuclear surface. Msp300-PE and isoforms expressed from the same transcriptional promotor (Msp300-PG and -PM) are expressed most highly in the fat body compared to the expression of the other isoforms, indicating that these isoforms and the unique protein domains they encode may be responsible for assembly of the MTOC on the nuclear surface. Our data also indicate that Msp300-PE is sufficient to generate the ncMTOC on the nuclear surface. Msp300-PE organizes the microtubules through recruitment of shot as well as Patronin, a major regulator of microtubules at the perinuclear MTOC [26], and is consequently required for nuclear positioning and endocytic vesicle trafficking in fat body cells. These findings explain why Msp300, expressed from a complex locus with expression in many cell types, organizes an ncMTOC on the surface of nuclei in a cell-type specific manner.

The knockdown of Msp300-PE/PG, or their disruption together with Msp300-PM with transposon insertions, indicates that Msp300-PE and -PG organize the perinuclear MTOC in fat bodies. The loss of Msp300-PG, together with all KASH-containing isoforms, reduced the MTs at the MTOC, but did not appear to significantly block its function, as nuclear positioning and the localization of Rab5-GFP were not significantly affected. Thus, we infer from all the results that Msp300-PE is sufficient to organize the MTOC, while Msp300-PG contributes.

In contrast with the majority of the other Msp300 isoforms, and Nesprins generally across species, Isoform E lacks the characteristic KASH domain and the abundant spectrin repeats. Also, we show that loss of all KASH-containing isoforms does not affect the MTOC in the fat body or the localization of Msp300 to the nuclear surface. However, KASH-less isoforms have been identified for other Nesprins in *Drosophila* and other species including *Drosophila* Klar, vertebrate Nesprin-1/2, and C. elegans ANC-1. A KASH-less isoform of Klar was shown to be associated with lipid droplets [42, 43]. In addition, KASH-less splice variants of Nesprin-1 and Nesprin-2 have been characterized [44-46], and an isoform of Nesprin-1 lacking the KASH domain was discovered in mice, where it was found in the early brain [47]. A Nesprin-1-giant isoform lacking the KASH domain has been identified in the CNS and is associated with spinocerebellar ataxia [48, 49]. Moreover, In *C. elegans*, ANC-1 regulates nuclear positioning in hypodermis syncytia independently of the KASH domain and the LINC complex [50]. Furthermore, while in *Drosophila* loss of the 5' isoforms was lethal at the first instar larval stage, deletion of the KASH domain from all isoforms was viable [31]. In *Drosophila* muscle, however, Msp300 was shown to be required for nuclear positioning in a KASH-dependent manner [18].

Despite the similarities with other KASH-less isoforms, Isoform E is particularly unique due to the presence of the two types of highly conserved ~100 amino acid-long tandem repeats. Based on the results of a protein BLAST against all insects, the repeats appear to possess significant homology only among *Drosophila* species. The repeats of Msp300 are predicted to contain β-sheets with disordered "linker" regions. This disorder may reflect a relatively weakly-folded structure, which may allow for elasticity and a spring-like role of Msp300. Msp300 may require elasticity in providing the connection between microtubules and the nucleus. Furthermore, the repeats are characterized by an overall negative charge, as observed in intrinsically disordered regions (IDRs) and intrinsically disordered proteins (IDPs) [51, 52]. The negatively charged regions may also facilitate binding with other proteins.

For example, the positively charged regions of Patronin, which bind to the negatively charged regions of MTs, may also interact with the repeats of Msp300.

Overall, this work shows that Msp300-PE has unique function to generate a perinuclear ncMTOC. Future work will elucidate the functions of the unique domains and how Msp300-PE is able to generate an ncMTOC on the surface of nuclei.

268 ## Materials and Methods

269 ***Drosophila* stocks**

270 Relevant information for each *Drosophila* stock is contained in Supplementary Table 1. Flies were
271 raised using standard food made of cornmeal, molasses, and yeast and were maintained at 25°C. Unless
272 otherwise specified, RNAi-based crosses were incubated at 25°C overnight prior to being transferred to
273 29°C to improve the efficiency and reduce the lethality of the knockdown.

274 **Generation and expression of FLP-FRT and coinFLP stocks**

275 The generation of FLP-FRT mutant clones was conducted by crossing y^1 *w* hsFLP*^{22}; Ubi-RFP-nls
276 neoFRT40A females to males with each *Msp300* allele recombined with neoFRT40A. For each cross, 30-
277 40 females were used.

278 The generation of coinFLP mosaic RNAi knockdowns was conducted using an adaptation of the
279 coinFLP system [27]. For each cross, 25-35 females of the genotype *w* hsFLP*^{1} *coinFLP-GAL4*^{attP3};; UAS-
280 mCherry-nls3 were crossed to RNAi line males.

281 Crosses were established for at least 2-3 days before proceeding with embryo collection and
282 recombination. Embryos were collected from FLP-FRT and coinFLP crosses for 2-3 h, and then embryos
283 were aged past the cleavage stage at 29°C for 2 hr. Embryos were then heat-shocked in a 37°C water
284 bath for 30 minutes and then returned to 29°C for coinFLP crosses or 25°C for FLP-FRT crosses.

285 **Sample preparation and immunostaining**

286 Fat bodies from late third-instar wandering larvae were dissected in 1× Dulbecco's phosphate-
287 buffered saline (D-PBS) (GIBCO, Waltham, MA, USA) as previously described [26]. Samples were
288 transferred to a poly-L-lysine-coated slide and fixed in 15 µL of 4% paraformaldehyde (PFA) for 8 min.
289 Next, a siliconized coverslip was placed on the slide and the sample was gently flattened and then flash
290 frozen in liquid nitrogen. Fat bodies from two larvae were used for each slide. The slides were stored in
291 1× PBS (137 mM NaCl, 2.7 mM KCl, 8.0 mM Na_2HPO_4, and 1.4 mM KH_2PO_4) prior to application of a
292 hydrophobic ring around the sample. Fat bodies were permeabilized, blocked, and stained in 100 µL of
293 staining solution (1× PBS, 1% BSA, 0.1% saponin) for 2 hr at RT or overnight at 4°C using the antibodies
294 and dyes listed in Supplementary Table 2. Slides were extensively washed in 1× PBS following staining.
295 Samples were mounted in 10 µL of mounting medium (80% glycerol, 0.1 M Tris pH 8.8, 0.05% p-
296 phenylenediamine dihydrochloride (Sigma, cat. no. P1519)) and stored at -20°C.

297 **Image acquisition**

298 Fat bodies were imaged with either a Nikon A1 or Nikon AX laser scanning confocal microscope
299 (Nikon, Japan). Specimens were imaged using a 60× oil-immersion objective with a 1.49 numerical
300 aperture (NA). Images were captured with the Nikon NIS-Elements AR software (version 4.6 or 5.42 with
301 Nikon A1 or Nikon AX, respectively) with 0.5 µm between *z*-sections. All images are presented as
302 maximum intensity projections of the *z*-stack.

303 **Quantification analysis**

Microscopy images were quantified using Fiji [53]. Perinuclear localization was calculated from a single *z*-slice, while nuclear mispositioning was calculated from a maximum intensity projection. Quantification of perinuclear localization was performed by creating multiple ROIs of the same size throughout the perinuclear region and averaging the total fluorescence intensity of each ROI. The background for each cell was accounted for by subtracting the value of an ROI in the cytoplasm from the value of the perinuclear region. For samples utilizing the coinFLP system, the value for each clone was depicted as ratio of the clone to an adjacent wild-type control cell. For all other samples, the average value of the clones from a slide was divided by the average value of the corresponding w^{1118} control slide. Quantification of nuclear positioning was conducted as previously described [26]. In brief, the coordinates of the cell or nuclear centroid were obtained by defining the boundary of the plasma membrane or nucleus, respectively. Next, the distance between the two coordinates was calculated.

RT-qPCR

For preparation of whole fly and flight muscle RNA, 10 adult flies were used. Ovary RNA was extracted from 10 adult virgin female flies. Brains and fat bodies were dissected from 10 late third-instar wandering larvae.Tissues were washed in 1× D-PBS following dissection. After homogenizing sample via pellet pestle and aspiration with a 20 G needle, RNA was isolated from all samples using TRIzol (Ambion, Austin, TX, USA) following the recommended protocol from the manufacturer. RNA from each sample was resuspended in water and the entire volume was treated using the TURBO DNA-*free* kit (Thermo Fisher, Waltham, MA, USA). cDNA was produced using the SuperScript IV (Invitrogen, Waltham, MA, USA) kit with oligo dT primers. Quantitative PCR was performed using the primer pairs shown in Figure 1A along with those for the *αTub84B* [54] and *Gpdh1* reference genes. Primer sequences are listed in Supplementary Table 3. Amplification and quantification was performed using the Brilliant III Ultra-Fast qPCR Master Mix (Agilent, Santa Clara, CA, USA). Quantification was performed using the $2^{-\Delta\Delta Ct}$ method. The expression levels of the 5' and E, G, M isoforms were compared to the average expression levels of All isoforms amplified from two separate primer pairs.

Statistics and reproducibility

For microscopy image calculations, three slides, with each containing the fat bodies from two larvae, were imaged. On each slide, ≥ 5 wild-type and ≥ 5 clone cells were included in the quantitation. The use of the mosaic systems in this study provided an internal control, which reduces variability arising from sample preparation. For non-mosaic tissues, 10 cells from each slide were quantified. Nuclear positioning and perinuclear localization values are expressed as the mean ± standard error of the mean (SEM). All samples for RT-qPCR were dissected in triplicate and each reaction was performed in triplicate. The data were significant based on a P-value < 0.05. For datasets with negative control samples, a one-way ANOVA was performed, while a one sample *t*-test was used for all other datasets. GraphPad Prism 10 (Dotmatics, Boston, MA, USA) was used for all analyses.

Acknowledgements

We thank Véronique Morel, Bénédicte Durand, Talila Volk, Michael Welte, and the Bloomington *Drosophila* Stock Center for *Drosophila* stocks; Talila Volk and the Developmental Studies Hybridoma Bank for antibodies; and Yue Julia Wang for assistance with RT-qPCR. We are grateful to Bloomington *Drosophila* Stock Center (NIH P40OD018537), Vienna *Drosophila* Resource Center [55], and FlyBase [56]

for curating indispensable tools and resources. Thank you to Batory Foods for their generous donation of fly food reagents to support this work.

This work was supported by NIH grant R01GM139971 to T. Megraw, and National Natural Science Foundation of China grant (32370731) and Shenzhen Science and Technology Program grant (JCYJ20230807091308018) to Y. Zheng.

References

1. Crisp M, Liu Q, Roux K, Rattner JB, Shanahan C, Burke B, et al. Coupling of the nucleus and cytoplasm. The Journal of Cell Biology. 2006;172(1):41-53. doi: 10.1083/jcb.200509124.
2. Horn HF, Brownstein Z, Lenz DR, Shivatzki S, Dror AA, Dagan-Rosenfeld O, et al. The LINC complex is essential for hearing. J Clin Invest. 2013;123(2):740-50. Epub 20130125. doi: 10.1172/JCI66911. PubMed PMID: 23348741; PubMed Central PMCID: PMCPMC3561815.
3. Mejat A, Misteli T. LINC complexes in health and disease. Nucleus. 2010;1(1):40-52. Epub 2011/02/18. doi: 10.4161/nucl.1.1.10530. PubMed PMID: 21327104; PubMed Central PMCID: PMCPMC3035119.
4. Storey EC, Fuller HR. Genotype-Phenotype Correlations in Human Diseases Caused by Mutations of LINC Complex-Associated Genes: A Systematic Review and Meta-Summary. Cells. 2022;11(24):4065. Epub 20221215. doi: 10.3390/cells11244065. PubMed PMID: 36552829; PubMed Central PMCID: PMCPMC9777268.
5. Zhang Q, Bethmann C, Worth NF, Davies JD, Wasner C, Feuer A, et al. Nesprin-1 and -2 are involved in the pathogenesis of Emery Dreifuss muscular dystrophy and are critical for nuclear envelope integrity. Hum Mol Genet. 2007;16(23):2816-33. Epub 20070829. doi: 10.1093/hmg/ddm238. PubMed PMID: 17761684.
6. Puckelwartz MJ, Kessler EJ, Kim G, Dewitt MM, Zhang Y, Earley JU, et al. Nesprin-1 mutations in human and murine cardiomyopathy. J Mol Cell Cardiol. 2010;48(4):600-8. Epub 20091124. doi: 10.1016/j.yjmcc.2009.11.006. PubMed PMID: 19944109; PubMed Central PMCID: PMCPMC2837775.
7. Stroud MJ. Linker of nucleoskeleton and cytoskeleton complex proteins in cardiomyopathy. Biophys Rev. 2018;10(4):1033-51. Epub 20180604. doi: 10.1007/s12551-018-0431-6. PubMed PMID: 29869195; PubMed Central PMCID: PMCPMC6082319.
8. Gros-Louis F, Dupre N, Dion P, Fox MA, Laurent S, Verreault S, et al. Mutations in SYNE1 lead to a newly discovered form of autosomal recessive cerebellar ataxia. Nat Genet. 2007;39(1):80-5. Epub 20061210. doi: 10.1038/ng1927. PubMed PMID: 17159980.
9. Wang JY, Yu IS, Huang CC, Chen CY, Wang WP, Lin SW, et al. Sun1 deficiency leads to cerebellar ataxia in mice. Dis Model Mech. 2015;8(8):957-67. Epub 20150505. doi: 10.1242/dmm.019240. PubMed PMID: 26035387; PubMed Central PMCID: PMCPMC4527285.
10. Attali R, Warwar N, Israel A, Gurt I, McNally E, Puckelwartz M, et al. Mutation of SYNE-1, encoding an essential component of the nuclear lamina, is responsible for autosomal recessive arthrogryposis. Human Molecular Genetics. 2009;18(18):3462-9. doi: 10.1093/hmg/ddp290.
11. Lawrence KS, Tapley EC, Cruz VE, Li Q, Aung K, Hart KC, et al. LINC complexes promote homologous recombination in part through inhibition of nonhomologous end joining. J Cell Biol. 2016;215(6):801-21. Epub 20161212. doi: 10.1083/jcb.201604112. PubMed PMID: 27956467; PubMed Central PMCID: PMCPMC5166498.
12. Warren DT, Tajsic T, Porter LJ, Minaisah RM, Cobb A, Jacob A, et al. Nesprin-2-dependent ERK1/2 compartmentalisation regulates the DNA damage response in vascular smooth muscle cell ageing. Cell Death Differ. 2015;22(9):1540-50. Epub 20150306. doi: 10.1038/cdd.2015.12. PubMed PMID: 25744025; PubMed Central PMCID: PMCPMC4532777.
13. Burke B. LINC complexes as regulators of meiosis. Current Opinion in Cell Biology. 2018;52:22-9. doi: 10.1016/j.ceb.2018.01.005.
14. Koszul R, Kim KP, Prentiss M, Kleckner N, Kameoka S. Meiotic chromosomes move by linkage to dynamic actin cables with transduction of force through the nuclear envelope. Cell. 2008;133(7):1188-201. doi: 10.1016/j.cell.2008.04.050. PubMed PMID: 18585353; PubMed Central PMCID: PMCPMC2601696.

15. Lee YL, Burke B. LINC complexes and nuclear positioning. Semin Cell Dev Biol. 2018;82:67-76. Epub 2017/12/02. doi: 10.1016/j.semcdb.2017.11.008. PubMed PMID: 29191370.
16. Rothballer A, Schwartz TU, Kutay U. LINCing complex functions at the nuclear envelope: what the molecular architecture of the LINC complex can reveal about its function. Nucleus. 2013;4(1):29-36. Epub 2013/01/18. doi: 10.4161/nucl.23387. PubMed PMID: 23324460; PubMed Central PMCID: PMCPmc3585024.
17. Zhang J, Felder A, Liu Y, Guo LT, Lange S, Dalton ND, et al. Nesprin 1 is critical for nuclear positioning and anchorage. Hum Mol Genet. 2010;19(2):329-41. Epub 20091028. doi: 10.1093/hmg/ddp499. PubMed PMID: 19864491; PubMed Central PMCID: PMCPMC2796894.
18. Elhanany-Tamir H, Yu YV, Shnayder M, Jain A, Welte M, Volk T. Organelle positioning in muscles requires cooperation between two KASH proteins and microtubules. The Journal of Cell Biology. 2012;198(5):833-46. doi: 10.1083/jcb.201204102.
19. Grady RM, Starr DA, Ackerman GL, Sanes JR, Han M. Syne proteins anchor muscle nuclei at the neuromuscular junction. Proc Natl Acad Sci U S A. 2005;102(12):4359-64. Epub 20050304. doi: 10.1073/pnas.0500711102. PubMed PMID: 15749817; PubMed Central PMCID: PMCPMC555524.
20. Puckelwartz MJ, Kessler E, Zhang Y, Hodzic D, Randles KN, Morris G, et al. Disruption of nesprin-1 produces an Emery Dreifuss muscular dystrophy-like phenotype in mice. Hum Mol Genet. 2009;18(4):607-20. Epub 20081113. doi: 10.1093/hmg/ddn386. PubMed PMID: 19008300; PubMed Central PMCID: PMCPMC2722216.
21. Zhang X, Xu R, Zhu B, Yang X, Ding X, Duan S, et al. Syne-1 and Syne-2 play crucial roles in myonuclear anchorage and motor neuron innervation. Development. 2007;134(5):901-8. Epub 20070131. doi: 10.1242/dev.02783. PubMed PMID: 17267447.
22. Volk T. A new member of the spectrin superfamily may participate in the formation of embryonic muscle attachments in Drosophila. Development. 1992;116(3):721-30. doi: 10.1242/dev.116.3.721. PubMed PMID: 1289062.
23. Wang S, Reuveny A, Volk T. Nesprin provides elastic properties to muscle nuclei by cooperating with spectraplakin and EB1. J Cell Biol. 2015;209(4):529-38. doi: 10.1083/jcb.201408098. PubMed PMID: 26008743; PubMed Central PMCID: PMCPMC4442817.
24. Folker ES, Baylies MK. Nuclear positioning in muscle development and disease. Front Physiol. 2013;4:363. Epub 20131212. doi: 10.3389/fphys.2013.00363. PubMed PMID: 24376424; PubMed Central PMCID: PMCPMC3859928.
25. Rey A, Schaeffer L, Durand B, Morel V. Drosophila Nesprin-1 Isoforms Differentially Contribute to Muscle Function. Cells. 2021;10(11):3061. Epub 20211106. doi: 10.3390/cells10113061. PubMed PMID: 34831284; PubMed Central PMCID: PMCPMC8616381.
26. Zheng Y, Buchwalter RA, Zheng C, Wight EM, Chen JV, Megraw TL. A perinuclear microtubule-organizing centre controls nuclear positioning and basement membrane secretion. Nat Cell Biol. 2020;22(3):297-309. Epub 20200217. doi: 10.1038/s41556-020-0470-7. PubMed PMID: 32066907; PubMed Central PMCID: PMCPMC7161059.
27. Bosch JA, Tran NH, Hariharan IK. CoinFLP: a system for efficient mosaic screening and for visualizing clonal boundaries in *Drosophila*. Development. 2015;142(3):597-606. doi: 10.1242/dev.114603.
28. Ni J-Q, Zhou R, Czech B, Liu L-P, Holderbaum L, Yang-Zhou D, et al. A genome-scale shRNA resource for transgenic RNAi in Drosophila. Nature Methods. 2011;8(5):405-7. doi: 10.1038/nmeth.1592.
29. Dietzl G, Chen D, Schnorrer F, Su K-C, Barinova Y, Fellner M, et al. A genome-wide transgenic RNAi library for conditional gene inactivation in Drosophila. Nature. 2007;448(7150):151-6. doi: 10.1038/nature05954.
30. Xu T, Rubin GM. Analysis of genetic mosaics in developing and adult Drosophila tissues. Development. 1993;117(4):1223-37. doi: 10.1242/dev.117.4.1223.

31. Technau M, Roth S. The Drosophila KASH domain proteins Msp-300 and Klarsicht and the SUN domain protein Klaroid have no essential function during oogenesis. Fly (Austin). 2008;2(2):82-91. Epub 20080301. doi: 10.4161/fly.6288. PubMed PMID: 18820478.
32. Xie X, Fischer JA. On the roles of the Drosophila KASH domain proteins Msp-300 and Klarsicht. Fly. 2008;2(2):74-81. doi: 10.4161/fly.6108.
33. Venken KJT, Schulze KL, Haelterman NA, Pan H, He Y, Evans-Holm M, et al. MiMIC: a highly versatile transposon insertion resource for engineering Drosophila melanogaster genes. Nature Methods. 2011;8(9):737-43. doi: 10.1038/nmeth.1662.
34. Bellen HJ, Levis RW, He Y, Carlson JW, Evans-Holm M, Bae E, et al. The Drosophila Gene Disruption Project: Progress Using Transposons With Distinctive Site Specificities. Genetics. 2011;188(3):731-43. doi: 10.1534/genetics.111.126995.
35. Sun T, Song Y, Dai J, Mao D, Ma M, Ni JQ, et al. Spectraplakin Shot Maintains Perinuclear Microtubule Organization in Drosophila Polyploid Cells. Dev Cell. 2019;49(5):731-47 e7. Epub 2019/04/23. doi: 10.1016/j.devcel.2019.03.027. PubMed PMID: 31006649.
36. Liem RK. Cytoskeletal Integrators: The Spectrin Superfamily. Cold Spring Harb Perspect Biol. 2016;8(10):a018259. Epub 20161003. doi: 10.1101/cshperspect.a018259. PubMed PMID: 27698030; PubMed Central PMCID: PMCPMC5046693.
37. Starr DA, Fischer JA. KASH 'n Karry: the KASH domain family of cargo-specific cytoskeletal adaptor proteins. Bioessays. 2005;27(11):1136-46. doi: 10.1002/bies.20312. PubMed PMID: 16237665.
38. Autore F, Pfuhl M, Quan X, Williams A, Roberts RG, Shanahan CM, et al. Large-Scale Modelling of the Divergent Spectrin Repeats in Nesprins: Giant Modular Proteins. PLOS ONE. 2013;8(5):e63633. doi: 10.1371/journal.pone.0063633.
39. Simpson JG, Roberts RG. Patterns of evolutionary conservation in the nesprin genes highlight probable functionally important protein domains and isoforms. Biochem Soc Trans. 2008;36(Pt 6):1359-67. doi: 10.1042/BST0361359. PubMed PMID: 19021556.
40. Morel V, Lepicard S, Rey AN, Parmentier ML, Schaeffer L. Drosophila Nesprin-1 controls glutamate receptor density at neuromuscular junctions. Cell Mol Life Sci. 2014;71(17):3363-79. Epub 20140204. doi: 10.1007/s00018-014-1566-7. PubMed PMID: 24492984.
41. Newman AM, Cooper JB. XSTREAM: a practical algorithm for identification and architecture modeling of tandem repeats in protein sequences. BMC Bioinformatics. 2007;8(1):382. Epub 20071011. doi: 10.1186/1471-2105-8-382. PubMed PMID: 17931424; PubMed Central PMCID: PMCPMC2233649.
42. Guo Y, Jangi S, Welte MA. Organelle-specific control of intracellular transport: distinctly targeted isoforms of the regulator Klar. Mol Biol Cell. 2005;16(3):1406-16. Epub 20050112. doi: 10.1091/mbc.e04-10-0920. PubMed PMID: 15647372; PubMed Central PMCID: PMCPMC551502.
43. Welte MA, Gross SP, Postner M, Block SM, Wieschaus EF. Developmental regulation of vesicle transport in Drosophila embryos: forces and kinetics. Cell. 1998;92(4):547-57. doi: 10.1016/s0092-8674(00)80947-2. PubMed PMID: 9491895.
44. Dawe HR, Adams M, Wheway G, Szymanska K, Logan CV, Noegel AA, et al. Nesprin-2 interacts with meckelin and mediates ciliogenesis via remodelling of the actin cytoskeleton. Journal of Cell Science. 2009;122(15):2716-26. doi: 10.1242/jcs.043794.
45. Rajgor D, Mellad JA, Autore F, Zhang Q, Shanahan CM. Multiple novel nesprin-1 and nesprin-2 variants act as versatile tissue-specific intracellular scaffolds. PLoS One. 2012;7(7):e40098. Epub 20120702. doi: 10.1371/journal.pone.0040098. PubMed PMID: 22768332; PubMed Central PMCID: PMCPMC3388047.
46. Zhang Q, Ragnauth CD, Skepper JN, Worth NF, Warren DT, Roberts RG, et al. Nesprin-2 is a multi-isomeric protein that binds lamin and emerin at the nuclear envelope and forms a subcellular network in skeletal muscle. J Cell Sci. 2005;118(Pt 4):673-87. Epub 20050125. doi: 10.1242/jcs.01642. PubMed PMID: 15671068.

47. Zhang X, Lei K, Yuan X, Wu X, Zhuang Y, Xu T, et al. SUN1/2 and Syne/Nesprin-1/2 complexes connect centrosome to the nucleus during neurogenesis and neuronal migration in mice. Neuron. 2009;64(2):173-87. doi: 10.1016/j.neuron.2009.08.018. PubMed PMID: 19874786; PubMed Central PMCID: PMCPMC2788510.

48. Razafsky D, Hodzic D. A variant of Nesprin1 giant devoid of KASH domain underlies the molecular etiology of autosomal recessive cerebellar ataxia type I. Neurobiol Dis. 2015;78:57-67. Epub 20150402. doi: 10.1016/j.nbd.2015.03.027. PubMed PMID: 25843669; PubMed Central PMCID: PMCPMC4426048.

49. Razafsky DS, Ward CL, Kolb T, Hodzic D. Developmental regulation of linkers of the nucleoskeleton to the cytoskeleton during mouse postnatal retinogenesis. Nucleus. 2013;4(5):399-409. Epub 20130823. doi: 10.4161/nucl.26244. PubMed PMID: 23974729; PubMed Central PMCID: PMCPMC3899130.

50. Hao H, Kalra S, Jameson LE, Guerrero LA, Cain NE, Bolivar J, et al. The Nesprin-1/-2 ortholog ANC-1 regulates organelle positioning in C. elegans independently from its KASH or actin-binding domains. Elife. 2021;10:e61069. Epub 20210416. doi: 10.7554/eLife.61069. PubMed PMID: 33860766; PubMed Central PMCID: PMCPMC8139857.

51. Uversky VN. Intrinsically Disordered Proteins and Their "Mysterious" (Meta)Physics. Front Phys-Lausanne. 2019;7:10. doi: 10.3389/fphy.2019.00010. PubMed PMID: WOS:000458061300001.

52. Wang X, Bigman LS, Greenblatt HM, Yu B, Levy Y, Iwahara J. Negatively charged, intrinsically disordered regions can accelerate target search by DNA-binding proteins. Nucleic Acids Res. 2023;51(10):4701-12. doi: 10.1093/nar/gkad045. PubMed PMID: 36774964; PubMed Central PMCID: PMCPMC10250230.

53. Schindelin J, Arganda-Carreras I, Frise E, Kaynig V, Longair M, Pietzsch T, et al. Fiji: an open-source platform for biological-image analysis. Nat Methods. 2012;9(7):676-82. Epub 2012/06/30. doi: 10.1038/nmeth.2019. PubMed PMID: 22743772; PubMed Central PMCID: PMCPMC3855844.

54. Jorgensen V, Chen J, Vander Wende H, Harris DE, McCarthy A, Breznak S, et al. Tunable Transcriptional Interference at the Endogenous Alcohol Dehydrogenase Gene Locus in Drosophila melanogaster. G3 (Bethesda). 2020;10(5):1575-83. Epub 20200504. doi: 10.1534/g3.119.400937. PubMed PMID: 32213532; PubMed Central PMCID: PMCPMC7202008.

55. Dietzl G, Chen D, Schnorrer F, Su KC, Barinova Y, Fellner M, et al. A genome-wide transgenic RNAi library for conditional gene inactivation in Drosophila. Nature. 2007;448(7150):151-6. Epub 2007/07/13. doi: 10.1038/nature05954. PubMed PMID: 17625558.

56. Öztürk-Çolak A, Marygold SJ, Antonazzo G, Attrill H, Goutte-Gattat D, Jenkins VK, et al. FlyBase: updates to the Drosophila genes and genomes database. Genetics. 2024;227(1). doi: 10.1093/genetics/iyad211.